A novel non-contact method for monitoring the Acoustic Emission from mixed EHL contacts

S. Hutt, A. Clarke, H.P. Evans

1 Abstract

Lubricated non-conformal contacts, such as between gear teeth, operate with high levels of mixed lubrication, where the amount of direct asperity contact depends on operating parameters which influence the film thickness. Understanding of the levels of surface interaction is key to optimising component life, and there is considerable interest in sensitive monitoring methods such as Acoustic Emission (AE). Researchers have shown that AE can detect subtle changes in lubrication conditions, using sensors mounted directly on the rotating gears. However, the use of such sensors is complex and unsuitable for implementation in real gearboxes. The alternative, of using sensors placed on housings, is hampered by signal attenuation and noise. This paper presents a novel, non-contact stationary sensor, coupled by an oil film to the rotating gear, which is shown to be capable of detecting important changes in lubrication conditions with significantly higher consistency and precision than housing-mounted sensors, whilst avoiding the complexities of gear-mounted sensors.

2 Definitions

a	Major semi-dimension of Hertzian contact ellipse
AAE	Asperity Acoustic Emission. The AE caused by asperity interactions in mixed EHL.
ADC	Analogue to Digital Conversion
AE	Acoustic Emission
CRS	Clamped Rotating AE Sensor
CRS-AAE	AAE measured by the CRS
CV	Contact Voltage
EHL	Elastohydrodynamic Lubrication
FD	Fast test disk
h	Lubricant film thickness for smooth surface EHL
HS	Housing AE Sensor
HS-AAE	AAE measured by the HS
OCSS	Oil-Coupled Stationary Sensor
OCSS-AAE	AAE measured by the OCSS
P_o	Maximum Hertzian contact pressure
RMS	Root Mean Square
R_q	RMS surface roughness
SRR	Slide Roll Ratio, $v_s/\bar{u}$
STD	Standard Deviation
u	Surface speed
$\bar{u}$	Entrainment speed, $(u_1 + u_2)/2$
v_s	Sliding speed, $\lvert u_1 - u_2 \rvert$
α	Pressure coefficient of viscosity
θ	Temperature in °C
Λ	Mixed lubrication parameter. Ratio of film thickness to composite surface roughness, $h/\left({R_{q1}}^2 + {R_{q2}}^2\right)^{1/2}$
μ_0	Absolute viscosity at zero pressure

3 Introduction

Acoustic Emission (AE) has long been established as a viable method for monitoring the condition of a wide range of structures and machines. In recent years, the advantage of AE as a highly sensitive tool to investigate the conditions at tribological contacts has been recognised. AE has been applied to monitor the condition of a wide range of machine elements, as diverse as blades, bearings and gearboxes in renewable energy devices [1], journal bearings [2], piston rings and cylinder liners in internal combustion engines [3], and in tribological tests [4,5]. In particular, its use to monitor lubricated contacts in gears and bearings has been widely researched. These concentrated contacts often operate under conditions of mixed lubrication, where the surface roughness is on the same scale as the Elastohydrodynamic Lubrication (EHL) film, with the result that the contact load is carried partly by direct asperity contact, and partly by a pressurised lubricant film. The degree of mixed lubrication is indicated by Λ, this is the ratio of the smooth surface film thickness (usually estimated numerically) to the RMS of the roughness heights (usually measured). The authors have previously demonstrated the effectiveness of AE at monitoring gear-like contacts operating in the mixed lubrication regime via a series of disk machine experiments, showing AE's sensitivity both to Λ and to incipient micropitting [6,7].

This sensitivity has meant that AE is an attractive tool for monitoring gears and gearboxes. Many researchers have conducted tests to investigate the effects of operating conditions on the AE generated at gear tooth contacts. As the gear operating conditions (speed, load, temperature, lubricant viscosity) directly affect the lubricant film thickness, and hence the amount of asperity interaction occurring, a clear link with AE levels has been observed, with researchers attributing increased AE to increased levels of direct asperity interaction [8-12]. Hamel *et al.* [8] induced gross changes of gear bulk temperature using liquid nitrogen. This therefore increased the viscosity of the entrained lubricant film, and they attempted to correlate the measured AE signals with film thickness. Further work by the same group [12] also used liquid nitrogen to induce film thickness changes in spur gears under test, and found a significant increase in RMS levels of AE as the EHL film thickness was decreased. However, given the Λ levels encountered, it was unlikely that asperity interaction was the *sole* mechanism of AE generation seen in these tests. Further experiments on spur and helical gears [9, 10], identified both a similar dependence of AE on Λ, and a further dependence on operating speed, together with some insight into the sources of continuous and burst AE seen within measured signals. Vicuna [11] conducted tests on planetary gear sets, and established a relationship between film thickness and RMS AE. Common to all of these papers, seeking to establish detailed information on the relationship between AE and lubrication film conditions, as well as the authors' previous works using disk machine experiments to undertake similar investigations [6, 7], is the fact that the sensors were always placed on the gears, near to the gear teeth themselves. Clearly this leads to a very effective source-sensor transmission path, with low levels of attenuation, but comes with the associated challenges of getting signals from the sensors to the AE instrumentation. Often, this is achieved by using expensive, high-quality slip rings.

Other workers have used AE to investigate further aspects of gear failure mechanisms, such as pitting. Many have used seeded defects, despite it not necessarily being the case that the AE signature from a seeded defect, produced by machining or otherwise damaging the gear before testing, will bear relation to the AE occurring as a defect grows naturally. For example, Eftekharnejad and Mba [13] were able to observe the effect of defects seeded onto gear teeth using a small drill when examining the AE waveforms recorded, and found a relationship between RMS AE and the volume of material removed. That said, workers from the same group [14] identified the difficulties in using seeded defects to mimic the behaviour of naturally-occurring defects, in a project that used sensors on both

the rotating gear and on the gearbox housing. They also noted that the attenuation seen by sensors mounted on stationary components was significant and presented challenges when compared to using sensors on the rotating gears. Novoa and Vicuna [15] investigated seeded defects on a planetary gearbox, and were able to identify defects in the planet and sun gears using AE.

Recognising the difficulties associated with seeded defect experimentation, many workers have investigated the AE from naturally-occurring defects in gear endurance tests. For example, Sentoku [16] and Scheer et al. [17] used AE to detect pitting, primarily using sensors mounted on the gears themselves. In comparative tests of AE and vibration on gear endurance experiments, it was generally found that AE out-performed vibration measurements, facilitating earlier detection of defects whilst they were at a smaller size [18, 19].

Noting the practical limitations of on-gear sensors [20], researchers have also compared the effectiveness of sensors mounted directly on the rotating gears with those mounted in more practical locations for industrial adoption of AE technology, typically on bearing or gearbox housings. For example, Toutountzakis and Mba [21] conducted tests using a back to back gearbox rig, with sensors on both the driven gear wheel and the bearing housing. They were able to detect damage using both sensor locations, but observed that the bearing housing signals were more complex, less clear and more heavily attenuated. Caso et al. [22] also compared on-shaft and bearing housing AE sensors, in experiments designed to investigate misalignment in low-speed gearboxes. They found that on-shaft AE was required to overcome the challenges of severe attenuation over multiple boundaries and distance faced by AE sensors mounted on stationary parts of the gearbox. Whilst there have been studies solely using sensors mounted on the gearbox housing [23], the majority of workers have found the complex transmission path and high attenuation between on-gear AE source and on-housing AE sensor difficult to overcome, as discussed by Sikorska and Mba [24] and Singh et al. [25].

Of the relevant papers discussed so far, 15 have used on-gear sensors, connected via slip ring or inductive transmission to the AE instrumentation. Of those 15, 5 have also collected signals using sensors mounted on gearbox or bearing housings. A further 3 papers solely used housing-mounted sensors. The prevalence of on-gear sensors demonstrates that, in order to obtain useful insight into contact conditions for gears using AE, it is highly useful to measure the AE as close as possible to the source, and to avoid the complex transmission paths and high levels of attenuation associated with stationary sensors. However, the majority of these papers were also laboratory based test-rig studies, as opposed to studies using real gearboxes in real applications, where there are strong drivers against the complexity and risk introduced by placing sensors on rotating gears and introducing slip rings or other costly equipment in order to transmit the signals from sensor to instrumentation. There have been some notable studies into methods to avoid these issues. For example, there are laser-based non-contact methods for measuring high-frequency vibrations, as used by Goyal et al. [26] to study rolling-element bearings. However to use such a system internally within a gearbox would be hampered by oil sprays and mists, for example. Loutas et al. [27, 28] developed a stationary AE sensor which was mounted on a steel cylinder, which was pressed against the side-face of the gear by a spring. This sliding contact allowed the transmission of AE from the gear to the sensor, and their work showed that the effects of frictional AE generated at the sliding sensor/gear face contact were sufficiently small to allow the identification of large changes in operating conditions and relatively severe gear tooth defects.

This paper presents a novel non-contact AE sensor system for monitoring the AE generated at mixed-lubrication contacts, typical of those found in heavily-loaded power-transmission gearing. Its effectiveness is demonstrated in disk machine experiments by comparison with AE sensors mounted on-disk and on a bearing housing. The novel stationary sensor is coupled using an oil film to the

rotating disk, and is shown to be capable of detecting the subtle changes in AE generated by asperity interactions within the contact – these have previously been investigated by the authors using sensors mounted on the rotating component near to the contact [6, 7]. It is proposed that this sensor design offers many of the benefits of on-gear sensing, with none of the drawbacks of complexity and cost, potentially improving the attractiveness of AE for monitoring of lubrication health in real gear systems.

4 Method

4.1 Disk rig

Test contact

The experiments took place on a rig which generates an EHL contact between the cylindrical surfaces of two test disks. This is a common approach to testing heavily-loaded contacts without the complications of varying kinematics and loading found within real gear or roller bearing contacts [29]. The disks' geometry and surface finish are designed to simulate contact between helical gear teeth. Figure 1 shows a photo of the contact surface of a used test disk. The disks have a face width of 9.53 mm (3/8") but are gently crowned so that an elliptical contact is generated[1]. The contact ellipse has an aspect ratio of 1:4 with the minor axis aligned with direction of entrainment. The darker region of surface in Figure 1 indicates the running track. The disks are made of case-hardened steel and are finished with a special grinding process [30] that generates the crown and imparts roughness with an axial lay. The RMS roughness R_q is typically between 0.3 and 0.5 µm depending on the extent of running-in and wear. Detailed analysis of the disks' roughness topography and its effects on the contact conditions can be found in the authors' previous work [31, 6].

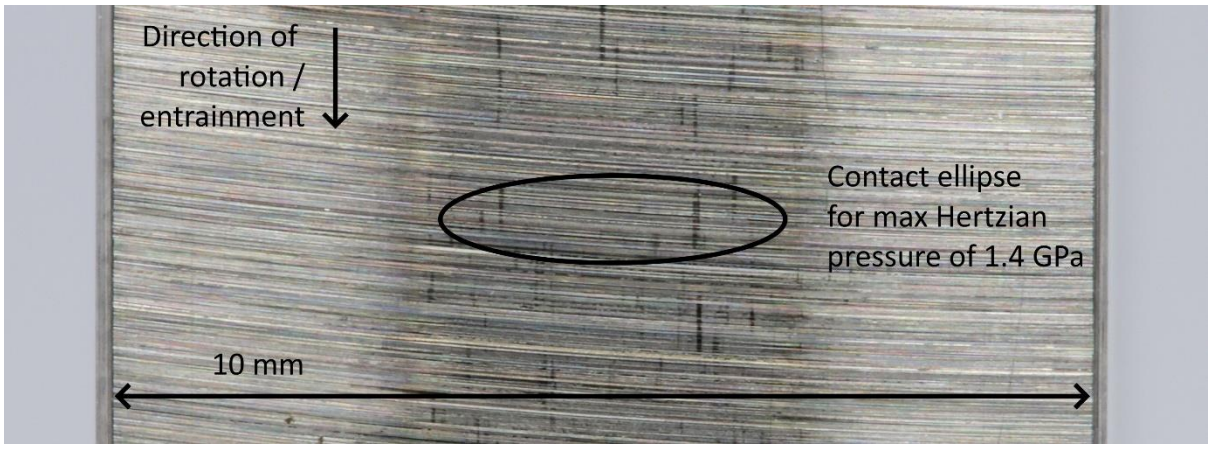

Figure 1. Photo of the contact surface of a test disk.

General rig specifications.

The disks are mounted on parallel shafts linked by a helical gear pair. The gear ratio determines the amount of sliding at the contact. The disks have identical diameters, so that when the gear ratio is unity there is no sliding, i.e. the disks rotate at the same speed in pure rolling. More commonly, a non-unity gear ratio is used so the disks rotate at different speeds. In such cases the contact consists of both rolling and sliding as indicated by the Slide Roll Ratio (SRR). The rig is driven by a variable speed

[1] Technically the contact surfaces are ellipsoidal rather than cylindrical.

induction motor. One disk shaft is supported in a pivot that allows the disks to move into and out of contact. In the no-load state the disks are separated at the contact, and a hydraulic ram is used subsequently to bring the disks into loaded contact. The contact is lubricated by OEP-80 gear oil [32], the viscosity and pressure coefficient of viscosity of which are given in Table 1.

Table 1. OEP-80 gear oil properties.

Temperature (°C)	μ_0 (Pa.s)	α (10^{-8}m^2/N)
40	0.065	1.99
100	0.008	1.29
35 to 120	~ $4.34\theta^{-2.37}$	~ $2.61e^{-0.00702\theta}$

The oil is pumped from a temperature-controlled bath and jetted directed into the contact inlet and outlet to maintain fully flooded lubrication conditions. The temperature of each disk is measured by a thermocouple embedded in a hole 3 mm below the contact surface. The temperature signals are wired through slip rings at the ends of each shaft. Further details of the rig design and principles of operation can be found in [6, 7].

Measurement of the lubrication conditions.

There are several control variables on the rig which can be used to vary the lubrication conditions. These are: the rotational speed, SRR, load, oil temperature, and disk surface finish. Three methods are currently used to determine the lubrication conditions. These are:

- Calculation of the Λ ratio.
- Measurement of the Contact Voltage (CV) across the disks.
- Measurement of the AE from asperity interactions in the test contact.

The AE measurement is the main subject of this paper and is described in detail in the next section. The other two methods are now described briefly.

The Λ ratio.

Λ is the ratio of oil film thickness for an equivalent smooth surface contact and the statistical roughness of the contact surfaces. If Λ is close to or below unity, it indicates that the surface roughness asperities are on the same scale as the oil film thickness. In this case they are likely to cause large transient pressure spikes in the oil film as they pass close to opposing asperities, or penetrate the film completely in direct contacts. This regime is termed mixed lubrication. If Λ is far above unity it indicates that the oil film will be thick enough to prevent any close-passes or direct contacts. This regime is termed full-film lubrication.

The roughness of the disks is measured using a stylus profilometer. Each disk can be measured in-situ (whilst assembled in the rig) to avoid disturbing the contact position, and the procedure is described in detail in [6, 33]. The oil film thickness of the test contact cannot be measured directly but is approximated using a formula developed by Chittenden and Dowson *et. al.* [34] for the central film thickness. Their formula was derived from numerical contact simulations and has been validated against optical interferometry measurements. The formula does not incorporate the thermal effects of operating conditions (SRR, speed and load) on the oil properties (viscosity and pressure coefficient of viscosity). Instead, the instantaneous oil properties are calculated from continuous measurement of the near-surface disk temperatures made using the thermocouples. There will be some measurement related error as the thermocouples cannot measure the contact flash temperature

(which would be impractical). For all experiments compared in this paper the influence of frictional heating at the contact on the bulk disk temperature and enclosure temperature was minor compared to heating by the lubricating oil, which heated the disks uniformly. Thus, the temperature difference between the test contact and the thermocouple position, and associated error, is assumed to have remained reasonably constant.

The roughness of the disks is measured using a stylus profilometer. Each disk is measured in-situ (whilst assembled in the rig) and the in-situ procedure is described in detail in [6, 33]. This ensures that the precise alignment between asperities on the two disks is not disturbed. The continuously determined oil film thickness is divided by the average disk roughness, measured before and after running, to determine the Λ ratio. The procedure for measuring and calculating Λ is described in more detail in [7].

The CV

The CV is a measure of the electrical resistance across the contact. It gives an indication of the amount of direct asperity contact. In full-film lubrication the oil electrically isolates one disk from the other, the contact will be effectively open-circuit and the CV will be that of the voltage source. In mixed-lubrication, instances of direct asperity contact form transient conduction paths across the contact causing the resistance and CV to decrease. In aggressive lubrication conditions the instances of direct asperity contact can be sufficiently numerous to provide continual near-zero resistance and CV. On the rig, one disk is electrically isolated using insulating couplings and bearings. An open-circuit voltage of 45 mV is applied to the other disk, and the CV is measured using a potential divider circuit. The CV measurements are normalised by the open-circuit voltage. Thus, a CV of unity indicates the lubrication regime is at or near full-film and lower values indicate that the lubrication regime is mixed. The point at which the CV decreases to zero does not indicate a physical limit of the lubrication regime, merely the limit of CV measurement range. Beyond this point it is entirely possible for the lubrication regime to become more aggressive, but the CV cannot detect this. As discussed in [7], one of the advantages of AE over CV is its increased measurement range and proportional response to the degree of mixed lubrication. Further details on the CV measurements, and how they relate to the lubrication conditions can be found in [33].

4.2 AE

Instrumentation

Three AE sensors were used in the experiments, the Oil-Coupled Stationary Sensor (OCSS), the Clamped Rotating Sensor (CRS), and the Housing Sensor (HS). The OCSS is the main focus of this paper, as it tests the novel oil-coupling method which this paper validates. The other two sensors use well established coupling methods and placements and are used for verification and comparison.

Figure 2 shows the shaft assemblies and the sensor couplings. (The two shaft assemblies are shown sectioned so that all components are visible). All sensors were of the same type: Physical Acoustics Corporation (PAC) 200-750 kHz Pico. This type was chosen for its small size, which was necessary due to space restrictions, as it has a face diameter of ~5 mm.

OCSS

The novel OCSS was held by a rigid arm next to, but not touching, one side of the fast disk. The sensor was wired directly to a pre-amplifier. Oil was jetted directly into the gap between the OCSS and the disk side to acoustically couple them. The sensor was positioned adjacent to the test contact to minimise signal attenuation. The sensor arm consisted of three orthogonal beams. These were bolted

together using slots so that position of the sensor could be adjusted during assembly. The arm was attached to the rig using two different methods.

For the first attachment method the arm passed through a gap in the enclosure wall and was affixed to a linear stage that moved parallel to axes of the disks. The linear stage was manually actuated by a micrometer dial and gauge. This allowed fine differential adjustment of the coupling thickness (the distance between the disk and sensor faces). An absolute coupling thickness was intended to be set by first butting the sensor face against the disk and then backing it off by the desired amount. However, in practice this did not work well as there was too much flex in the arm to identify a distinct 'first-contact' position. Another drawback of this attachment method was that the linear stage was also required for making in-situ surface roughness measurements of the disks. Whenever this was done the sensor position was lost and had to be reset. Roughness measurements were typically made before and after each change in test parameter (e.g., load, speed etc.) and so ensuring a consistent sensor position across these changes was not possible.

For the second attachment method the arm was directly bolted to the inside of the enclosure wall, this is the method shown in Figure 2. The arm was not disturbed during surface roughness measurements so a consistent sensor position could be maintained. The coupling thickness was set by placing shims in-between the sensor and disk, butting the sensor against the shims and then tightening the bolts in an axially aligned slot. This method was used for most experiments presented here.

CRS

The CRS was clamped directly to the other side of the fast disk. A grub screw applied the clamping pressure and silicone rubber was used in the interface to fill any surface roughness voids. As this sensor was rotating, the signal was wired through a silver-graphite slip-ring before connection to a pre-amplifier. The quality of measurements from the CRS has been established previously [6,7]. The signal quality is high, possibly best-case, due to the close proximity of the source and sensor, and the stability and low attenuation of the coupling. The downside is the requirement for a slip-ring, which the OCSS addresses.

HS

The HS was glued using epoxy to the housing of the fast shaft bearing located farthest from the drive gears. The bearing was a cylindrical roller and the sensor was positioned at the position of maximum roller loading (e.g. coincident with the radial load line). This sensor was wired directly to a pre-amplifier. The transmission path from the fast disk to this sensor involved the following five interfaces in order: disk to shaft (press fit), shaft to inner raceway (press fit), inner raceway to cylindrical rollers (EHL), cylindrical rollers to outer raceway (EHL), and outer raceway to housing (split clamp). The HS was used as a comparison to test the need for the novel OCSS. Both types can be wired directly (without slip-ring), but the HS is significantly easier to implement. Thus, if their measurement quality was similar, the HS would be the preferred choice.

Conditioning and AAE

The signals from each sensor were conditioned identically. The pre-amplifiers had a gain of 40 dB and a 20 kHz high-pass analogue filter. The signals were logged at an ADC rate of 2 or 5 MHz depending on the experiment. For short stages (several minutes maximum) the signals were logged continuously but for longer stages the signals were logged periodically and synchronised with the rotational frequency.

In [6,7] measurements from the CRS were used to identify signals components from asperity interactions in the test contact. It was found that the RMS of the 150 – 300 kHz passband varied in

proportion with the amount of asperity interactions, this parameter was termed the Asperity Acoustic Emission (AAE). In this paper a further distinction is necessary, the AAE as measured by each different sensor, these are termed the OCSS-AAE, CRS-AAE and HS-AAE respectively.

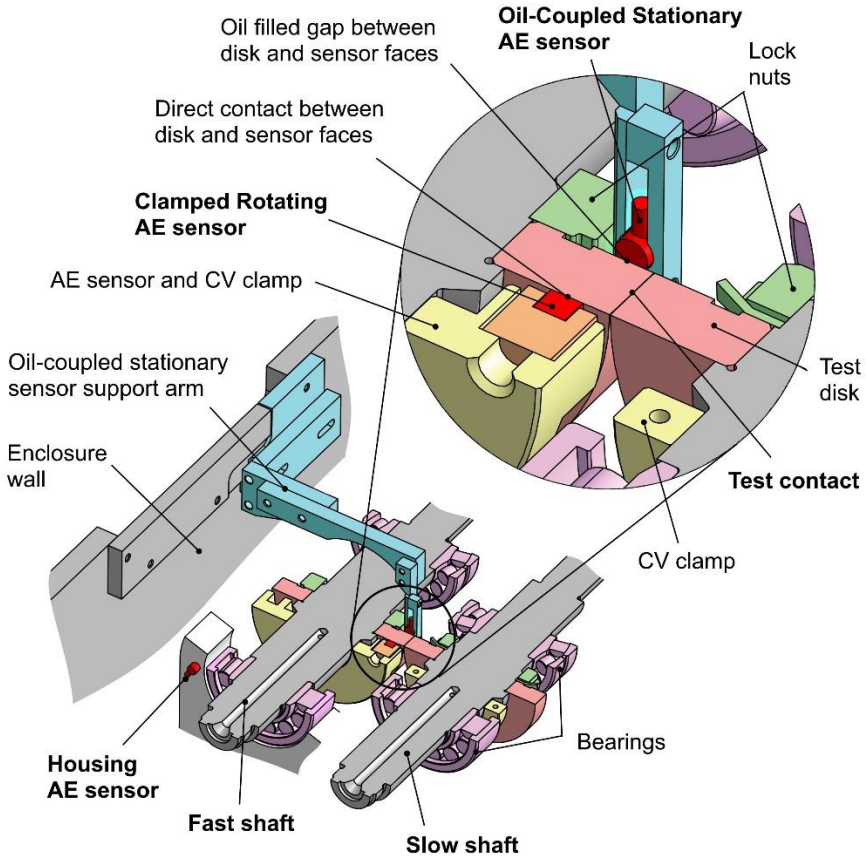

Figure 2 AE sensor locations and fixtures.

5 OCSS attenuation

When the OCSS was first installed on the rig a simple experiment was carried out to assess the effect of the oil coupling thickness on the signal attenuation. With the sensor arm affixed to the linear stage, a series of 60 second test stages were run. In-between each, the coupling thickness was incremented from near-zero to approximately 1 mm. ('Near-zero' corresponds to the smallest definite clearance between disk and sensor detectable by eye). All subsequent coupling thicknesses were set as offsets from this. (Surface roughness measurements were not made in-between test stages so that the near-zero reference was maintained). The test parameters are shown in Table 2 and were chosen to ensure mixed-lubrication conditions. During each stage the disk temperatures increased by ~5°C due to frictional heating, this caused a decrease in Λ from 0.84 to 0.74. Mixed-lubrication conditions were confirmed by CV measurements. The OCSS-AAE and CRS-AAE were measured continuously during each stage. In addition, they were measured shortly before and after each stage, when the disks were running at the test-speed but under no load.

Table 2. Test parameters for OCSS attenuation tests (to 2 s.f.)

Load	1.3 kN
SRR	0.25

$\bar{u}$	3.5 m/s
Disk temperatures	70 - 75 °C
Fast disk R_q	0.41 µm
Slow disk R_q	0.37 µm
Λ	0.84 – 0.74

Figure 3 shows the mean and standard deviation of the OCSS-AAE for each coupling thickness. Also shown are the mean OCSS-AAE from the no-load periods immediately before and after each stage, and the mean CRS-AAE during each stage.

The CRS-AAE remained approximately constant across all test stages, between 34 and 36 mV, indicating that the AAE generated by the test contact was stable. The no-load OCSS-AAE also remained approximately constant, just below 2 mV. This shows that the coupling itself did not generate any significant AE.

The OCSS-AAE decreased rapidly with increasing coupling thickness, indicating that signal attenuation is strongly dependent on the thickness of the oil coupling. Even at the near-zero position the amplitude of the OCSS-AAE was approximately three times less than that of the CRS-AAE. At an offset of 0.5 mm from the near-zero position, the OCSS-AAE had decreased to near that measured during the no-load condition and did not decrease further. This experiment demonstrates that a moving oil-coupling can effectively transmit AE and that minimising the coupling thickness is important to maximise signal strength.

Based on the results of this experiment, all subsequent OCSS measurements were made using the arm that attached directly to the enclosure wall (as shown in Figure 2) and with an oil coupling thickness set to 0.2 mm using shims. This thickness was selected as a compromise between attenuation and the risk of the sensor contacting the disk in extreme operating conditions.

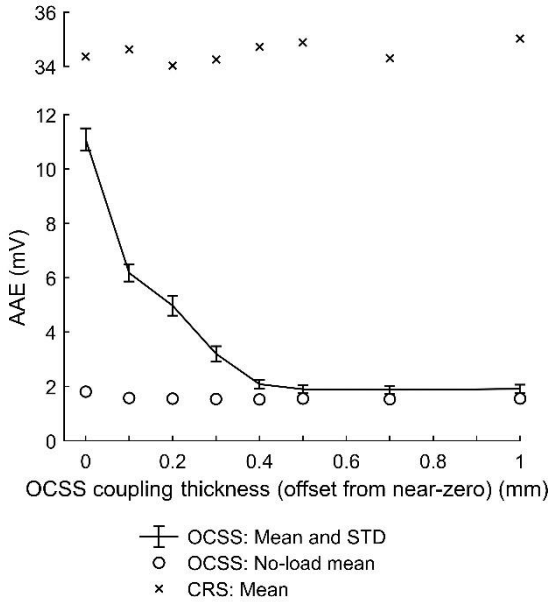

Figure 3. Mean AAE vs. OCSS coupling thickness. The error bars span ± one STD.

6 Film thickness experiments

6.1 Introduction

This section presents the AAE measurements from several experiments where temperature control was used to cause a decrease in oil film thickness and a transition from full-film to mixed lubrication.

6.2 Method

The measurements were made in a series of stages, Table 3 shows the schedule and parameters. (P_o is the maximum Hertzian contact pressure, *a* is the major semi-dimension of the contact ellipse). For each stage the rig was started from room temperature and then the oil was heated at constant power until it reached a temperature of ~110 °C at which point the stage was stopped. This took between 50 and 60 minutes. The SRR was 0.5 for all stages, the speed was constant during each stage. The load was not intentionally varied but decreased as the oil temperature increased[2]. The actual load was used in all calculations of film thickness. The load ranges in Table 3 correspond to the starting and ending load of each stage.

Speed stepping set B contains repeats of some of the stages in set A. It is included because the housing AE sensor was not present for set A. The AE sampling regimes were also different, set B consisted of much more infrequent but longer samples. (The regime was changed to provide data for a collaborative effort with international researchers developing a new 'cyclostationary' analysis technique [20]).

The experiments were carried out on a single pair of well-used disks which were fully run-in for all lubrication conditions tested. In-between each stage the disks' roughness profiles were measured. No significant wear was observed over the experiments with the roughness of the disks remaining stable. The fast disk roughness measured between 0.36 and 0.38 µm R_q, the slow disk between 0.34 and 0.36 µm R_q.

Table 3. Test schedule for the film thickness experiments

Experiment	Stage no.	$\bar{u}$ (m/s)	Load (kN)	P_o (GPa)	a (mm)	AE sensors	AE sampling
Speed stepping set A	1	0.96	1.7 to 1.5	1.26 to 1.21	1.58 to 1.52	OCSS CRS	5 MHz ADC every 25th FD rotation for period of one FD rotation.
	2	1.60					
	3	3.19					
	4	4.79					
	5	6.38					
Speed stepping set B	6	0.96				OCSS CRS HS	2 MHz ADC every 5 min for period of 10 s.
	7	3.19					
	8	6.38					
Load stepping	9	1.60	1.7 to 1.5	1.26 to 1.21	1.58 to 1.52		2 MHz ADC every 25th FD rotation for period of one FD rotation.
	10		0.85 to 0.55	1.00 to 0.88	1.26 to 1.09		
	11		0.43 to 0.14	0.80 to 0.55	1.00 to 0.69		

[2] This is a consequence of temperature variation in the oil used for the hydraulic ram. The rig uses a single oil supply for both lubrication and the ram. It was originally designed for experiments using a constant oil temperature where this would not have been a problem.

Figure 4 illustrates the effects of temperature on the lubrication conditions[3] with the stage 5 measurements. It presents the CRS-AAE, mean disk temperature and CV, vs. Λ. The figure can be read chronologically left to right. At the start of the stage the cold, viscous oil generated a relatively thick film. The CV was near unity and the CRS-AAE near its minimum indicating no significant asperity interactions and a full-film regime. As the temperature increased, the oil viscosity dropped causing the oil film to thin and Λ to decrease. Despite this, the CV and CRS-AAE initially remained constant as the film remained thick enough to effectively separate the opposing asperities. At a Λ value of ~4 the CRS-AAE began to increase exponentially and at a value of ~1.5 the CV began to abruptly decrease. These changes were the result of increasing asperity interactions / contacts and indicate a transition to mixed lubrication. By the time Λ decreased below unity both the CV and CRS-AAE were extremely sensitive to changes in Λ indicating that the lubrication was well within the mixed regime. The delayed response of the CV compared to the CRS-AAE is hypothesised to be due to their different sensitivity. AE is a stress / strain phenomenon and AE may be generated by pressure spikes resulting from close-passing asperities. In contrast the CV is unlikely to be affected by close-passes as only a very thin film of oil is needed to provide effective insulation. The CV only responds to the more extreme condition of direct asperity contact.

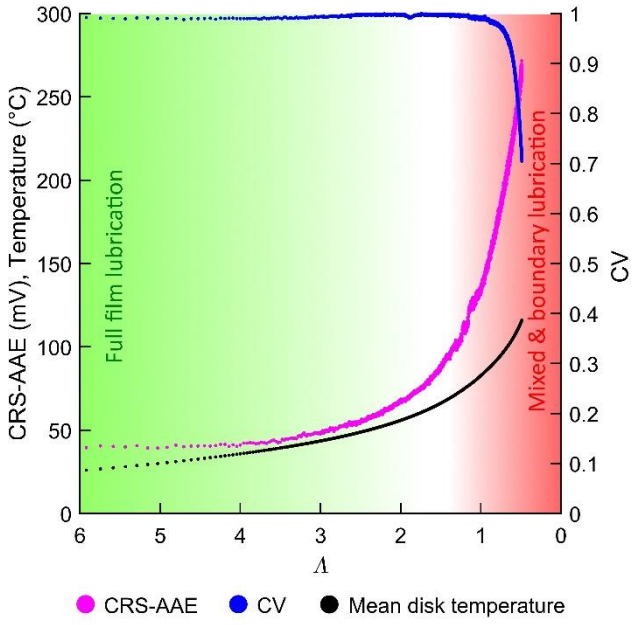

Figure 4. Lubrication measurements vs. Λ for test run no. 5.

6.3 Speed stepping set A

This section presents the CRS-AAE and OCSS-AAE measurements from speed stepping set A, test stages 1 to 5. The CRS-AAE results from this experiment have been previously published in detail in [7].

Figure 5 shows spectrograms of the broadband AE vs. Λ for test stage 3 ($\bar{u}$ = 3.19 m/s). Pane (A) shows the measurements from the OCSS and (B) the CRS, the AAE region of 0.15 - 0.3 MHz is indicated in both panes. The spectral distribution of the AE vs. Λ is broadly similar for both sensors. Across the

[3] Temperature change will affect how AE propagates through a material, but the authors have found that any such effects on the measured AAE amplitude to be negligible [7]. This was verified by testing continuously full-film lubrication conditions (using superfinished disks) over the temperature range of 30 – 110 °C. The measured AAE did not increase with temperature.

spectrum all the regions of activity in the CRS measurements are also present in the OCSS measurements.

In the OCSS spectrum there is pronounced AE activity in 0.45 - 0.6 MHz band which is not the case for the CRS spectrum. The 0.45 - 0.6 MHz band also contains AEE which is hypothesised to be a harmonic of the AEE in the 0.15 – 0.3 MHz band. The 0.45 – 0.6 MHz AEE was not used in the previous CRS investigation [7] as it was found to be more susceptible to obfuscation by noise. The quality between the two bands for the OCSS is more even, but the 0.15 - 0.3 MHz band is still superior. Thus, the comparisons in this paper use the AAE in the 0.15 - 0.3 MHz band.

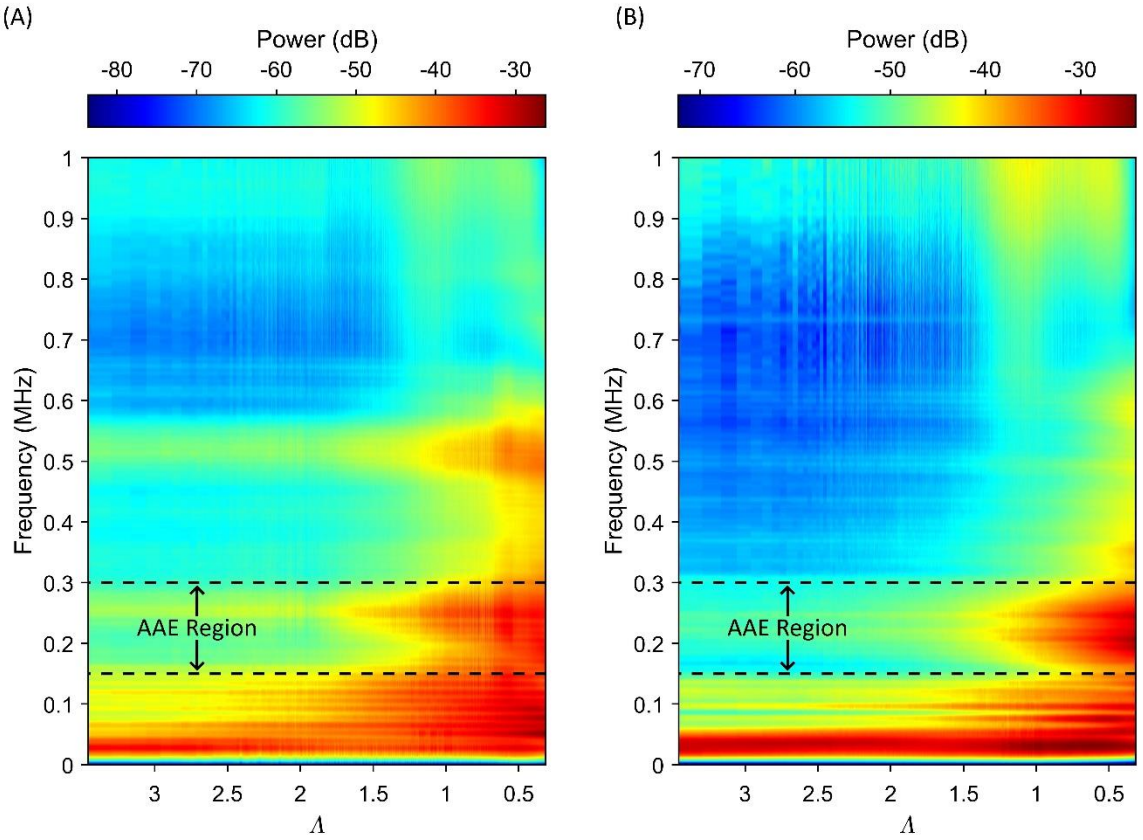

Figure 5. AE spectrograms for (A) the OCSS and (B) the CRS from test run no. 3 ($\bar{u}$ = 3.19 m/s).

Figure 6 presents the OCSS-AAE and CRS-AAE vs. Λ for the 5 test stages of speed stepping set A. The change in speed has two effects. First there is the effect of increased entrainment, this increases the oil film thickness, consequently shifting the Λ range of each speed step, from 0.15 – 1.26 for the slowest speed to 0.49 – 5.74 for the fastest. Despite this there is a Λ range that was covered by all speeds ~ 0.5 – 1. Secondly each speed increase 'amplified' the AAE signal. This can be seen by considering the AAE at constant Λ. For example at Λ equal to unity, the AAE magnitude increased by two orders of magnitude from the slowest to the fastest speed despite nominally equivalent amounts of asperity contact. This speed related AE 'amplification' has been observed in diverse experiments [3,12,35]. It is typical of AE generated from moving machinery and is hypothesised to occur because as the speed of a system increases, AE events occur with greater energy and over shorter timescales. More analysis of the speed amplification be found in [7] where the effect of Λ and speed on the CRS-AAE was empirically modelled.

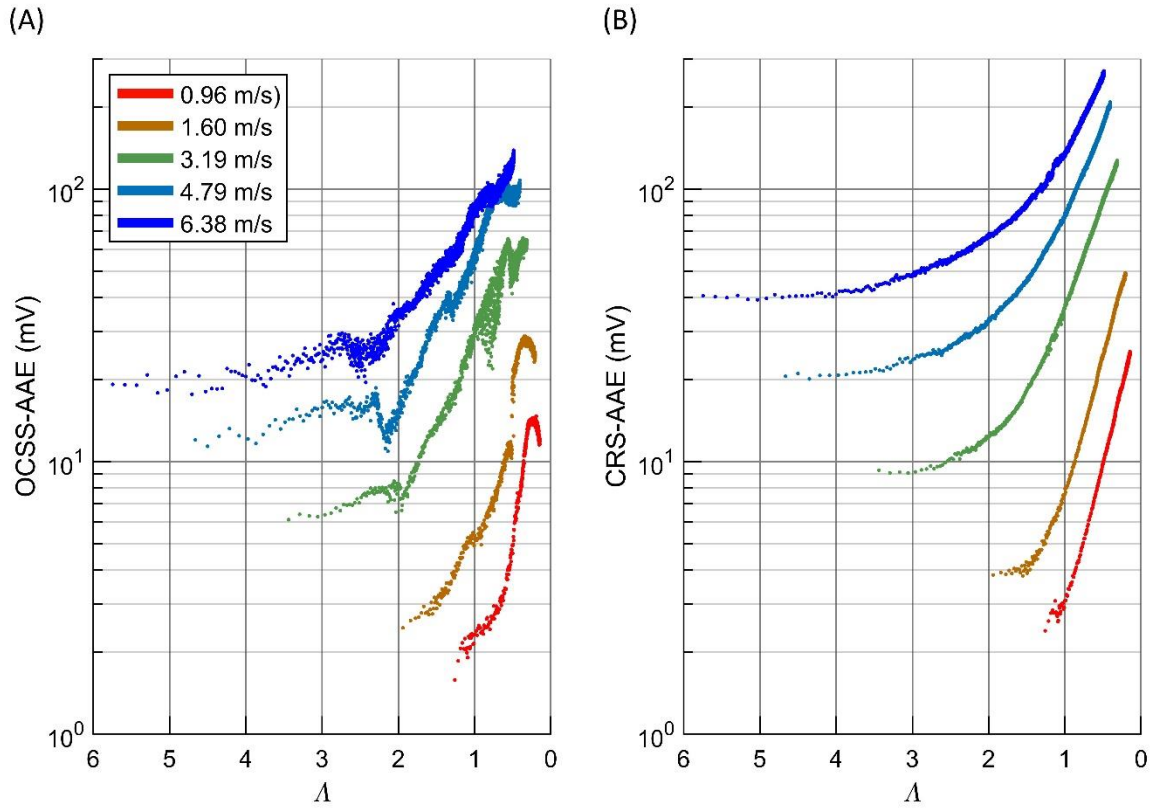

Figure 6. (A) OCSS-AAE vs. Λ and (B) CRS-AAE vs. Λ for all runs from the speed stepping experiment.

Stage 3 ($\bar{u}$ = 3.19 m/s) is now presented in more detail. Figure 7 presents the CRS-AAE and OCSS-AAE vs. Λ, for test stage 3 alone. It was shown in [7] that the relationship between CRS-AAE and Λ at constant speed could be accurately described by the following exponential model, where A, B and C are the fitting coefficients:

$$AAE = Ae^{-B\Lambda} + C \tag{1}$$

Fits of this model for test stage 3 ($\bar{u}$ = 3.19 m/s) are plotted in Figure 7 and the coefficients given in Table 4:

Table 4. Fits to the exponential model for test stage 3.

	Coefficients (to 3 s.f.)		
	A	*B*	*C*
CRS:	231	2.10	8.70
OCSS:	107	1.52	4.32

Figure 7 shows that as Λ decreased the CRS-AAE and OCSS-AAE behaved similarly. Both showed a transition from low to high sensitivity as Λ decreased and asperity interactions became increasingly significant. The results from both sensors satisfactorily fit the exponential model although the CRS-AAE has a much more precise fit, (so much so that in Figure 7 the samples are largely hidden behind the fit line). The amplitude of the OCSS-AAE is approximately half that of the CRS-AAE. (This is apparent in Table 4, where the linear scaling coefficients, *A* and *C,* for the OCSS are approximately half that of the CRS).

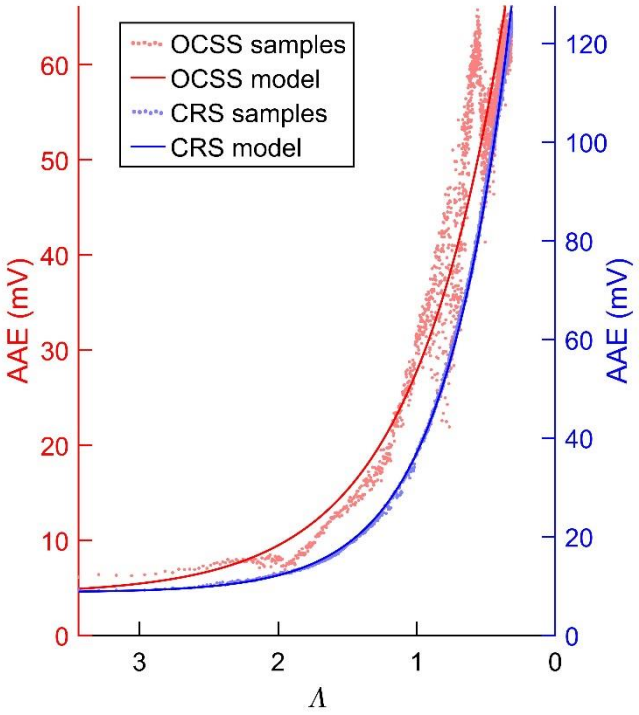

Figure 7. OCSS-AAE and CRS-AAE vs. Λ for test stage no. 3.

6.4 Speed stepping set B

Figure 8 presents plots of AAE vs. Λ for stage 7 ($\bar{u}$ = 3.19 m/s) of speed stepping set B. As previously mentioned, this stage was a repeat of stage 3 but with the inclusion of HS measurements and less frequent sampling. The AAE has been normalised by the maximum measured by each sensor. These maximums were 126, 58 and 1.5 mV for the CRS, OCSS and HS respectively. The maximums of the CRS-AAE and OCSS-AAE are consistent with the results of stage 3, Figure 7. The maximum of the HS-AAE is an order of magnitude less than that of the other two sensors. It can be seen that although housing sensor regisistered an increase in AAE when Λ decreased below ~0.75, above this value it was insensitive to Λ. In comparison, the other two sensors remained sensitive well above this value, indicating they could detect subtler asperity interaction. The lower sensitivity of the housing sensor is attributed to a much lower signal to noise ratio.

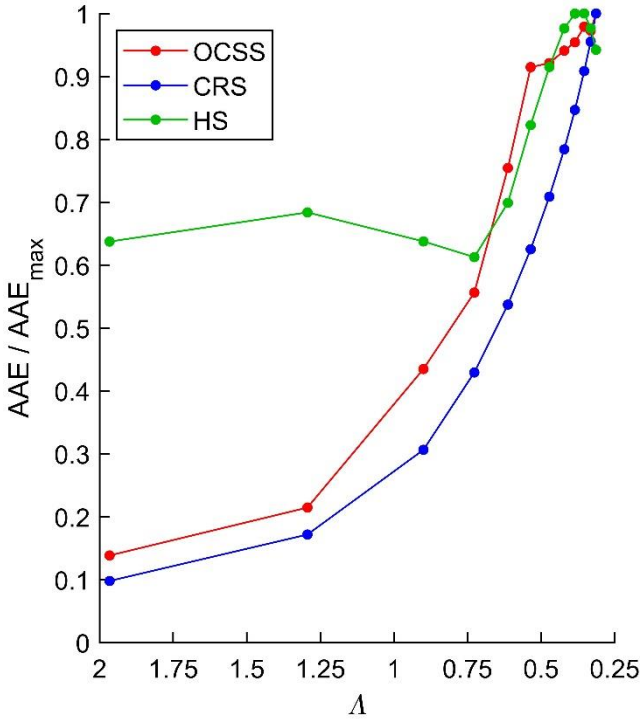

Figure 8. OCSS-AAE, CRS-AAE and HS-AAE vs. Λ for test stage no. 7.

6.5 Load stepping results.

This section presents the results of the load stepping experiment, test stages 6 to 9. Figure 9 shows the AAE vs. Λ as measured by (A) the OCSS, (B) the CRS, and (C) the HS. The OCSS and CRS measurements both show the expected increase in AAE at low Λ indicative of the transition to mixed lubrication. As with the speed stepping results, the amplitudes measured by the HS are an order of magnitude less than other sensors. An increase in HS-AAE at low Λ is still evident for the two lower loads but not the highest where the measurement does not correlate at all with the lubrication conditions. The reason for this is unclear, it may be the AE generated by the bearing contacts at the higher load is obscuring the AAE from the test disk, this remains to be investigated.

The effect of load on the relationship between CRS-AAE and Λ will now be examined. At relatively high Λ, the CRS-AAE appears to be nearly independent of load, it is approximately 5 mV for all three load cases. But as Λ decreases, the CRS-AAE increase is more pronounced with heavier loads. It is hypothesised that this is due to changes in the contact area. As the load increases so does the contact area, it follows that for equivalent film thickness conditions (i.e. constant Λ) the amount of asperity interactions will scale with area. Exploring this further, Figure 10 presents the AAE from both sensors vs. the Hertzian contact area at $\Lambda = 0.3$ (the AAE was calculated as the mean of values within the range $\Lambda = 0.3 \pm 0.0025$). Both sensors reveal a strong linear correlation between AAE and Hertzian contact area within the mixed regime.

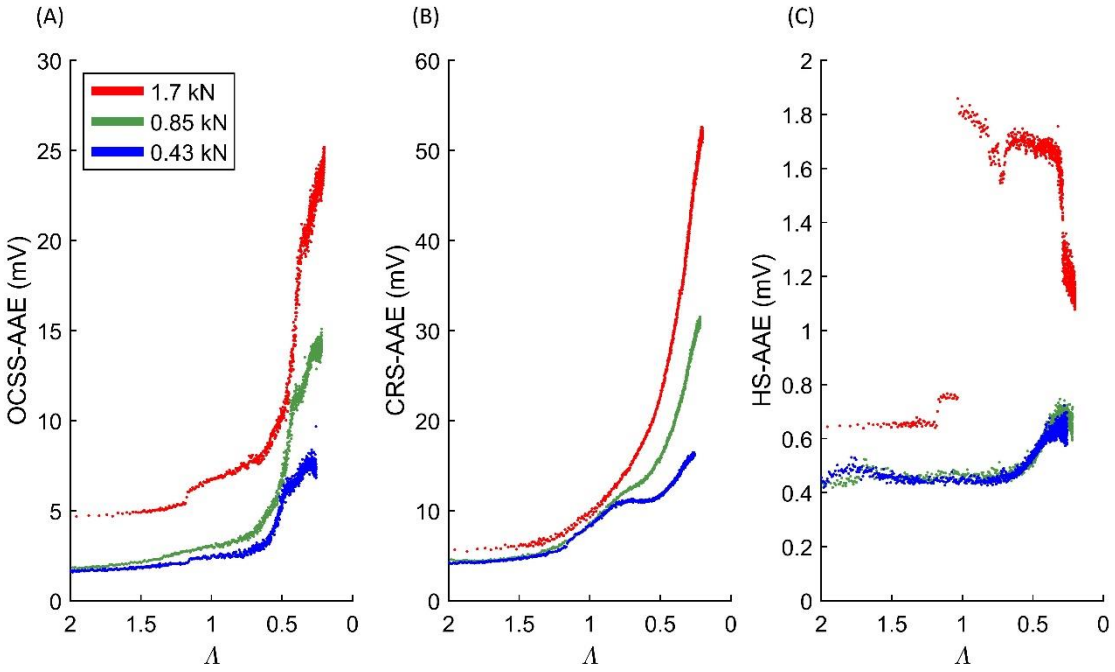

Figure 9. AAE vs. Λ for the load stepping experiment as measured by (A) the OCSS (B) the CRS and (C) the HS.

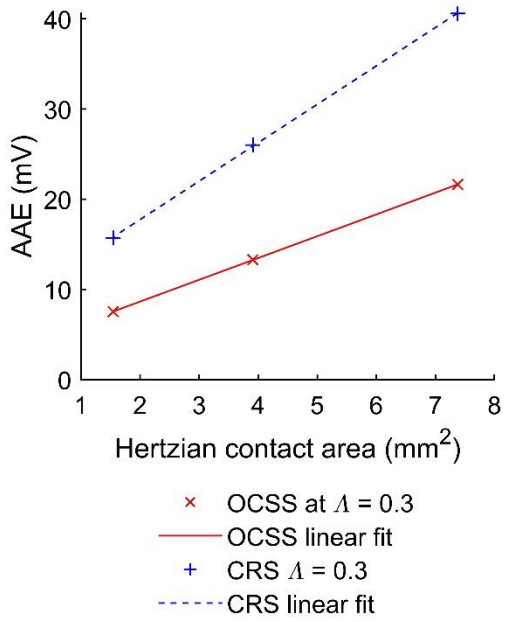

Figure 10. AAE at Λ = 0.3 vs. the Hertzian contact area for the OCSS and CRS measurements.

7 Wear experiment

7.1 Introduction

This section presents the OCSS-AAE and CRS-AAE measurements from an experiment where new test disks were allowed to run-in and wear (micropit) at otherwise constant contact conditions. The CRS-AAE measurements from this experiment have been previously discussed in detail in [6].

7.2 Method

New disks were installed in the rig and then run for a series of test stages in-between which the disk surfaces were measured for wear. Table 5 shows the contact parameters for the experiment, these were kept constant for all test stages. Unlike in the film thickness experiment, the oil was pre-heated and circulated through the rig prior to the start of each stage. This brought the disk temperatures up to that of the oil, so that when the stage started there was only a small further increase caused by frictional heating. After the start of each stage the disk temperatures quickly stabilised to between 85 and 95 °C depending on the stage. Once the temperature had stabilised the oil film thickness remained constant and so all subsequent changes to the mixed lubrication condition were caused by changes in surface roughness.

Table 5. Wear experiment contact parameters.

SRR	0.5
$\bar{u}$ (m/s)	3.2
Load (kN)	1.46
P_o (GPa)	1.20
a (mm)	1.51
Oil bath temperature (°C)	80

Table 6 shows the schedule for the wear experiment. Two relatively short stages were followed by 17 much longer ones. Previous experiments [6, 31] had shown that running-in of surface roughness took only tens of seconds or less. Thus, running-in was expected to be completed by the end of test stage 1. Test stage 2 was used to verify the completion of running-in by comparing the surface topography at the start and end of the stage, more details on this process can be found in [31]. Any wear after the initial running-in was anticipated to be slow to accumulate, so the subsequent stages were much longer. Initially they were set at a duration of 100 minutes each, but after the 13th stage, a cumulative running time of 22 hours, very little wear was occurring and so the remaining stages were lengthened to 300 minutes each.

Table 6. Wear experiment test schedule.

Test stages	Description	Duration per stage (min)	Fast disk cycles per stage
1	Running-in	3	3000
2	Running-in verification	3	3000
3 to 13	Long term wear testing	100	1 x 10^5
14 to 19	Long term wear testing	300	3 x 10^5

7.3 Running-in

Table 7 shows the in-situ R_q roughness measurements of the disks made before and after test stages one and two. The first test stage caused a relatively large decrease in roughness whereas the second did not. These measurements confirm that running-in occurred in the first stage and had ceased by its end.

Table 7. In-situ R_q roughness before and after test stages one and two.

Measurement	R_q, average of both disks, (µm)	Change in R_q, (µm)
Before test stage 1	0.448	-
After test stage 1	0.367	-0.082
After test stage 2	0.364	-0.003

Figure 11 presents the OCSS-AAE and CRS-AAE vs. time for the first two test stages. For these two test stages the AE signals were logged from before the load was applied until after it was removed so the loading / unloading ramps are included. (The disks were already running at test speed before the load was applied). In both panes of Figure 11 a time of one second corresponds to the approximate start of the load ramp.

As has been discussed in detail in [6], the CRS-AAE associated with running-in is revealed by the difference in the measurements of test stage one and two. This difference occurs at the very start of the stages, where there is a significant spike in CRS-AAE for the first but not the second. The spike is caused by the rapid running-in of surface asperities as they are deformed or fracture over several cycles. It is absent from the second stage as the roughness has already conformed to the test load.

The importance of this experiment for this paper is the equivalence between the OCSS-AAE and CRS-AAE. The running-in spike, and then its absence, is present in both measurements. In general, the response of the OSCS-AAE matches that of the CRS-AAE but with reduced amplitude (approximately $1/5^{th}$).

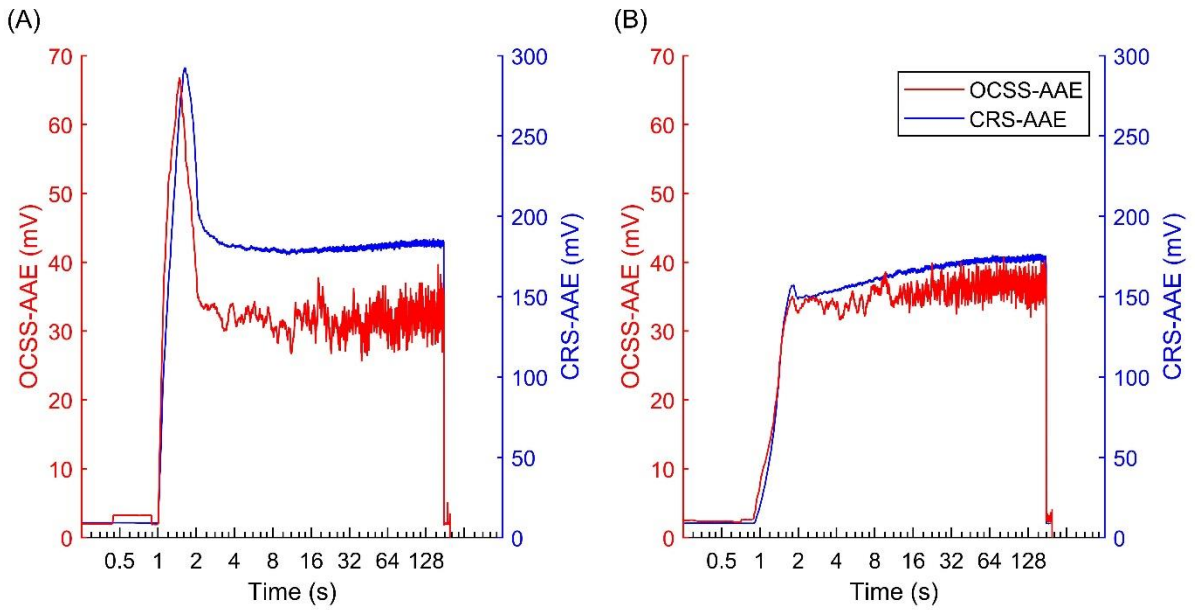

Figure 11. OCSS-AAE and CRS-AAE vs. time for (a) test stage 1 and (b) test stage 2.

7.4 Wear

Figure 12 presents the OCSS-AAE, CRS-AAE and in-situ R_q roughness vs. fast disk rotations for test stages 3 to 13. The division marks on the fast disk rotations axis indicate the start and end of the test stages. The R_q roughnesses, measured in-situ in between each test stage are the averages of both disks. The roughness decreased over the course of the experiment due to the removal of prominent asperities by micro-pitting (as verified by analysis of the roughness topography [6]). Consequently the CRS-AAE also decreased, as the micro-pitting reduced the amount of asperity interactions. Further details on the micro-pitting wear and its relationship with AAE can be found in [6].

The equivalence between the OCSS-AAE and CRS-AAE is not as clear as for the other experiments presented in this paper. Whereas the CRS-AAE decreased consistently with relatively smooth transitions from one test stage to the next, this was not the case for the OCSS-AAE. The OCSS-AAE amplitude fluctuates from one test stage to the next. For some test stages there was a significant jump in amplitude, this is most pronounced at 5 x 10^5 fast disk cycles where the following test stage had an amplitude 1.6 times that of the proceeding one. This is inconsistent with the lubrication conditions. The authors have considered possible causes, such as temperature (and thus film thickness) variation or disturbance to the rig in-between test stages. But there is no evidence to support them and so further investigation is required.

Despite the inconsistencies in-between some test stages there remains equivalence between the OCSS-AAE and CRS-AAE measurements on the scale of the entire experiment. The shift from relatively rapid change at the start to near steady state at the end is evident in both measurements and the ratio of final to starting amplitude is similar for both at approximately 0.3.

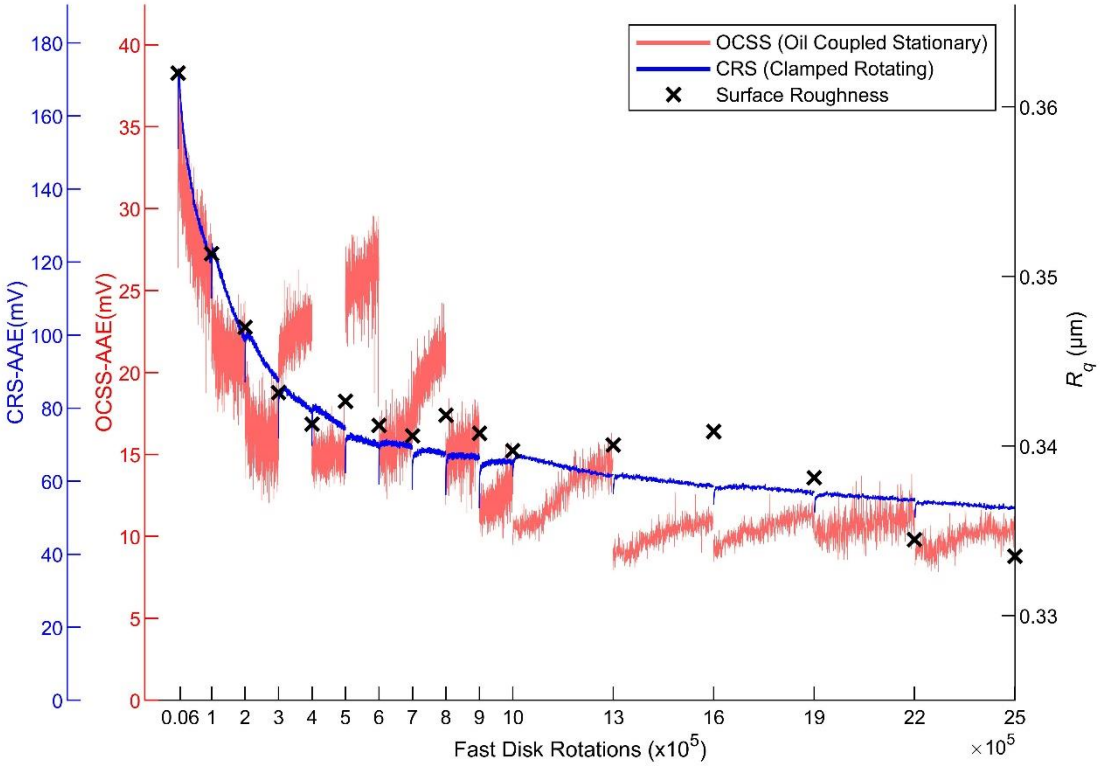

Figure 12. OCSS-AAE, CRS-AAE and in-situ R_q vs. fast disk rotations.

8 Discussion

By comparison with an established method of measuring the AE from a rotating component the experiments in this paper show that a stationary oil-coupled sensor is also a viable means of measurement. Considered broadly, the AAE as measured by the OCSS was consistent with lubrication theory and with measurements made by the CRS. In the mixed regime the OCSS-AAE was sensitive to changes in asperity interaction whether induced by changing film thickness or surface modification from running-in and micropitting.

For all the experiments presented here the amplitude response of the OCSS-AAE was less than the CRS-AAE, indicating that the oil coupling caused greater attenuation than the direct coupling. This is to be expected and is likely to be a characteristic of any oil coupled sensor. The greater attenuation was not a problem for the conditions tested here. Test stage 1 had the slowest speed, $\bar{u} = 0.96$ m/s, and because of this it generated the weakest AE signal. Nevertheless, the OCSS-AAE still clearly indicated a change in lubrication conditions caused by decreasing Λ (see Figure 6).

Regarding the quality of the measurements from the OCSS, it is evident that they are generally inferior to those from the CRS. Firstly, the precision is often less, as evident in many of the plots of AAE vs. Λ or time. In these plots the CRS-AAE datapoints have relatively little spread and form thin curves in contrast to the OCSS-AAE where the spread is often significant. (The clearest example of this is in the near-steady-state periods at the end of the two running-in test stages, Figure 11). Secondly, and more importantly, the accuracy of the measurements is inconsistent. Although the OCSS measurements are broadly equivalent with those of the CRS, and consistent with broad changes in lubrication conditions, this is not the case at the detailed level. Good examples of inconsistencies occur in test stages 1 and 2 of the film thickness experiment (Figure 6). In these, the OCSS-AAE increased significantly from the

start to finish as expected, however at the end of each stage there was a downturn which would seem to indicate an easing of the lubrication conditions despite decreasing Λ. This is inconsistent with the CRS-AAE measurements and the CV measurements. The downturn must be the result of an inaccuracy in the OCSS-AAE measurement at this point in the experiment.

The lower quality of the measurements from the oil coupling compared to the direct coupling is to be expected. Whereas the direct coupling remained stable despite changes in speed and temperature this is not true of the oil coupling. Lubricated contacts are sensitive to changes in speed and temperature and there are various factors which may have affected AE transmission and thus coupling accuracy. These include: the effects of oil viscosity on AE wave propagation; inconsistent oil flow, for example air bubbles; and changes in coupling thickness due to thermal expansion. The OCSS sensor was also more difficult than the CRS to assemble consistently. Due to the need for some adjustability of position it was difficult to ensure optimal and repeat positioning, and some parameters could only be checked by eye, skewness for example. For this reason, except for the attenuation tests, the OCSS was only adjusted / removed when the test disks were changed. The authors are currently developing a self-aligning version of the OCSS to address some of these issues.

As a first feasibility study, the oil coupling used for these experiments was relatively crude. It is now hoped that using lubrication theory it will be possible to refine the design of the coupling to improve its performance. One avenue of current investigation is the use of a loaded tilting pad arrangement to maintain a stable, self-aligning hydrodynamic wedge contact.

It is important to put the lower quality of the measurements of the OCSS compared to the CRS into context. In many applications it may not be practical or desirable to use slip rings or wireless power / transmission so a CRS would not be an option. In this situation the choice is between an oil coupling and a housing sensor. As shown by the results of these experiments the OCSS outperformed the HS both in terms of signal strength and consistency. In the speed stepping set B experiment (Figure 8) the HS was only able to detect changes to the lubrication conditions once well within the mixed regime whereas the OCSS was able to detect the prior transition from full-film to lightly mixed conditions. In the load stepping experiment (Figure 9) the performance of the HS was inconsistent, with a complete breakdown of capability for the highest load, in contrast the OCSS was consistent across all three stages.

Regarding the performance of the OCSS it is important to highlight that the changes in lubrication that were measured in these experiments were relatively subtle. For example, the surface modifications that precipitated the change in AAE over the wear experiment, Figure 12, were small and consisted only of slight ‘erosion’ of prominent asperities and sparse micro-pitting. The change in the statistical roughness, R_q, from start to finish was only -0.03 µm. Although a directly clamped sensor is likely to remain the preferred choice for academic investigations, where the highest quality measurements are sought, it is likely that the quality offered by an oil coupled sensor will be sufficient for many practical condition monitoring applications. Most importantly, the oil-coupled sensor offers a route to implementing AE in a meaningful way for the detailed health monitoring of lubricated contacts, whilst overcoming the barriers to implementation faced by directly clamped sensors.

It would be desirable to have an indication of when a lubrication regime is transitioning from full-film to mixed conditions as this has implications for surface life. As demonstrated in the film thickness experiments the OCSS-AAE can indicate this change. For example, using test stage three (Figure 7), even crude thresholds of OSCC-AAE < 10 mV, 10 mV ≤ OSCC-AAE ≤ 20 mV, and OSCC-AAE > 20 mV would provide an indication of whether the lubrication regime was full-film, uncertain / in-transistion, or mixed. Admittedly, that is a rather simplistic case: constant speed and load, and without the

complications of gear tooth contact cycles. Futhur research will be required to determin how the OSCC measurements can be used in more general lubrication monitoring.

It will be difficult to determine the lubrication conditions of an EHL contact from the AAE signal alone, as so many common operating variables act as 'amplification factors' on the AAE amplitude including speed and load, the effects of which have been demonstrated in this paper. For example, if presented with increasing AAE magnitude without any further context it would be very difficult to deterimine if the increase was the result of worsening lubrication conditions (more asperity contacts) or the effects of speed amplificaion which could increase AAE magnitude even with improving lubrication conditions. There are several methods that could be developed to address this difficulty.

The first method is to develop a 'digital twin' of the contact to be monitored. This would involve simulating the AAE from the expected operating conditions and comparing it to the measured AAE, any difference would indicate a potential lubrication problem. To simulate the AEE would likely require some empirical calibration for the particular system to be monitored, and knowledge of the contact temperature, load and speed. The authors have previously shown that it is possible to develop an empirical model that predicts the AAE based on oil viscosity (temperature) and speed [7], and are confident the model could be extended to cover other common variables such as load and SRR. For gears, the tooth meshing cycle adds a further complication but this can be addressed by averaging as demonstrated by [20].

The second method would treat the contact as a black-box AAE generator and use comparision data to monitor the lubrcation conditions. The current AAE pattern, generated over a period of time or operating condition, could be compared against a known healthy AAE pattern created at start-of-life, and any divergence would indicate a potential lubrication problem. This method would rely on general pattern recognition techniques and would not require a fundamental understanding of how the contact generates AE. It would be more suitable for situations where the contact parameters cannot be easily measured.

Finally, it should be noted that this paper has shown that the oil coupled sensor can detect changes within *healthy* lubrication regimes, i.e. relatively subtle changes. It is expected that it will be much easier to detect more extreme and damaging situations affecting the amount of asperity contact, e.g. oil starvation and scuffing.

9 Conclusions

This work has demonstrated a new method of sensor coupling that can be used to measure the AE from rotating transmission components such as gears, bearings, and shafts. It is concluded that:

- The AE from asperity contacts in mixed lubrication can be measured using a stationary non-contact AE sensor which is adjacent to the moving component and is coupled with an oil film. Using such a sensor it is possible to detect the transition from full-film to mixed lubrication conditions in a healthy gear-like contact under different speed and load conditions. These results imply that other events generating AE of similar or greater magnitude will also be detectable.
- The signal attenuation increases rapidly as the coupling film thickness increases. Nevertheless, it is not necessary to use very thin (EHL scale) films to provide acceptable transmission. The coupling film thickness used for the experiments in this paper was approximately 0.2 mm. It is likely that thicker films will be acceptable in situations where sensitivity does not need to be maximised.

- The signal strength measured by an oil coupled sensor will be less than that of a sensor clamped directly to the rotating component but significantly more than that of a housing sensor located 'downstream' of bearings. In situations where a directly clamped sensor is not feasible, an oil coupled sensor will be better suited to detecting subtle AE than a housing sensor.
- The quality of the measurements from a basic oil coupling are likely to be less than those of a directly clamped sensor but considerably better than those of a housing sensor. A directly clamped sensor provides the highest fidelity signal and can detect extremely subtle changes in lubrication conditions, such as the decrease in asperity contacts caused by sparse micro-pitting. The current design of oil coupling provides a less consistent and precise measurement but can still be used to detect the important change from full-film to mixed lubrication, which has important implications for surface wear. The oil coupled sensor was able to detect the change more consistently and earlier than the housing sensor.
- The oil-coupled sensor concept addresses many of the difficulties associated with other methods of mounting AE sensors – it does not require the slip rings associated with directly clamped on-gear sensors, neither does it face the complex transmission path and high attenuation levels associated with housing sensors. In short, it allows AE to be used to provide detailed insights into lubrication and surface finish conditions in heavily-loaded gear contacts in a way which is feasible for real-world applications.

10 Copyright statement

11 Acknowledgements

The authors wish to acknowledge the support of the EPSRC (Grant reference EP/L021757/1) which supported this work in part.

12 References

[1] He Y, Li M, Meng Z, Chen S, Huang S, Hu Y, Zou X. An overview of acoustic emission inspection and monitoring technology in the key components of renewable energy systems. Mechanical Systems and Signal Processing 2021: 148:107146.

[2] Poddar S and Tandon N. Study of Oil Starvation in Journal Bearing Using Acoustic Emission and Vibration Measurement Techniques. J. Tribol 2020;142(12);121801. doi: 10.1115/1.4047455.

[3] Douglas RM, Steel JAJ, Reuben RL. A study of the tribological behaviour of piston ring/cylinder liner interaction in diesel engines using acoustic emission. Tribol Int 2006;39:1634–42. doi:10.1016/j.triboint.2006.01.005.

[4] Kashyap A, Harsha AP, Rawat SS, Barshilia HC. Comparative Study on Galling and Antiwear Behaviour of Polyurethane Based Coatings Reinforced with Pristine and Alkylated MoS_2 Nanosheets. J. Tribol 2023;145(4);041401. doi: 10.1115/1.4056126.

[5] Lei Z, Zhu X, Li Y, Song Z, Liu H, Fu YQ. Characterization and Tribological Behaviour of TiAlN/TiAlCN Multilayer Coatings. J. Tribol 2018;140(5);051301. doi: 10.1115/1.4039723.

[6] Hutt S, Clarke A, Evans HP. Generation of Acoustic Emission from the running-in and subsequent micropitting of a mixed-elastohydrodynamic contact. Tribol Int 2018;119:270–80. doi:10.1016/J.TRIBOINT.2017.11.011.

[7] Hutt S, Clarke A, Pullin R, Evans HP. The acoustic emission from asperity interactions in mixed lubrication. Proc R Soc A Math Phys Eng Sci 2019;475:20180900. doi:10.1098/rspa.2018.0900.

[8] Hamel M, Addali A, Mba D. Investigation of the influence of oil film thickness on helical gear defect detection using Acoustic Emission. Applied Acoustics 2014, 79, 42-46.

[9] Raja Hamzah RI, Mba D. The influence of operating condition on acoustic emission (AE) generation during meshing of helical and spur gear. Tribol Int 2009, 42, 3-14.

[10] Tan CK and Mba D. Correlation between acoustic emission activity and asperity contact during meshing of spur gears under partial elastohydrodynamic lubrication. Trib Lett 2005, 20(1), 63-67.

[11] Vicuna CM. Effects of operating conditions on the Acoustic Emissions (AE) from planetary gearboxes. Applied Acoustics, 2013.

[12] Raja Hamzah RI, Al-Balushi KR, Mba D. Observations of Acoustic Emission Under Conditions of Varying Specific Film Thickness for Meshing Spur and Helical Gears. J Tribol 2008;130:021506 1-12. doi:10.1115/1.2908915.

[13] Eftekharnejad B and Mba D. Seeded fault detection on helical gears with acoustic emission. Applied Acoustics, 2009, 70, 547-555.

[14] Toutountzakis T, Tan CK, Mba D. Application of acoustic emission to seeded gear fault detection. NDT&E International, 2005, 38, 27-36.

[15] Novoa A B and Vicuna C M. New aspects concerning the generation of acoustic emissions in spur gears, the influence of operating conditions and gear defects in planetary gearboxes. Insight, 2016. DOI: 10.1784/insi.2016.58.1.18

[16] Sentoku H. AE in tooth surface failure process of spur gears. Progress in Acoustic Emission IX, 1998, S19-S24.

[17] Scheer C, Reimche W, Bach F-W. Early fault detection at gear units by acoustic emission and wavelet analysis. J. Acoustic Emission, 2007, 25, 331-340.

[18] Tan CK, Irving P, Mba D. A comparative experimental study on the diagnostic and prognostic capabilities of acoustics emission, vibration and spectrometric oil analysis for spur gears. Mechanical Systems and Signal Processing, 2007, 21, 208-233.

[19] Tandon N and Mata S. Detection of Defects in Gears by Acoustic Emission Measurements. J. Acoustic Emission, 1999, 17 (1-2), 23-27.

[20] Feng P, Borghesani P. Chang H, Smith WA, Randall RB, Peng Z. Monitoring gear surface degradation using cyclostationarity of acoustic emission. Mechanical Systems and Signal Processing, 2-19, 131, 199-221.

[21] Toutountzakis T and Mba D. Observations of acoustic emission activity during gear defect diagnosis. NDT&E International, 2003, 36, 471-477.

[22] Caso E, Fernandez-del-Rincon A, Garcia P, Iglesias M, Viadero F. Monitoring of misalignment in low speed geared shafts with acoustic emission. Applied Acoustics, 2020, 159, 107092.

[23] Wirtz SF, Beganovic N, Tenberge P, Söffker D. Frequency-based damage detection of spur gear using wavelet analysis. 8th European Workshop on Structural Health Monitoring (EWSHM 2016), 5-8th July 2016, Bilbao, Spain.

[24] Sikorska JZ and Mba D. Challenges and obstacles in the application of acoustic emission to process machinery. Proc. IMechE Part E: J. Process Mechanical Engineering, 2008, 222, 1-19.

[25] Singh A, Houser DR, Vijayakar S. Detecting Gear Tooth Breakage Using Acoustic Emission: a Feasibility and Sensor Placement Study. Journal of Mechanical Design, 1999, 121, 587-593.

[26] Goyal D, Vanraj, Pabla BS, Dhami SS. Non-contact sensor placement strategy for condition monitoring of rotating machine-elements. Engineering Science and Technology, an International Journal, 2019, 22, 489-501.

[27] Loutas TH, Kalaitzoglou J, Sotiriades G, Kostopoulos V. A Novel Approach for Continuous Acoustic Emission Monitoring on Rotating Machinery Without the Use of Slip Ring. Journal of Vibration and Acoustics, 2008, 130, 064502-1.

[28] Loutas TH, Roulias D, Pauly E, Kostopoulos V. The combined use of vibration, acoustic emission and oil debris on-line monitoring towards a more effective condition monitoring of rotating machinery. Mechanical Systems and Signal Processing, 2011, 25, 1339-1352.

[29] Prajapati DK and Tiwari M. Assessment of Topography Parameters During Running-In and Subsequent Rolling Contact Fatigue Tests. J. Tribol 2019;141(5);051401. doi: 10.1115/1.4042676.

[30] Patching MJ, Kweh CC, Evans HP, Snidle RW. Conditions for Scuffing Failure of Ground and Superfinished Steel Disks at High Sliding Speeds Using a Gas Turbine Engine Oil. J Tribol 1995;117:482–9. doi:10.1115/1.2831279.

[31] Clarke A, Weeks IJJ, Snidle RW, Evans HP. Running-in and micropitting behaviour of steel surfaces under mixed lubrication conditions. Tribol Int 2016;101:59–68. doi:10.1016/j.triboint.2016.03.007.

[32] Defence Standard 91-74, Lubricating Oil, Steam Turbine and Gear, Extreme Pressure Joint Service Designation: OEP-80. 2006.

[33] Clarke A, Weeks IJJ, Evans HP, Snidle RW. An investigation into mixed lubrication conditions using electrical contact resistance techniques. Tribol Int 2016;93:709–16. doi:10.1016/j.triboint.2014.10.010.

[34] Chittenden R., Dowson D, Dunn J., Taylor C. A Theroretical Analysis of the Isothermal Elastohydrodynamic Lubrication of Concentrated Contacts II. General case, with lubricant entrainment along either principal axis of the Hertzian contact ellipse or at some intermediate angle. Proc R Soc London A 1985;397:271–94. doi:10.1098/rspa.1939.0005.

[35] Cockerill A, Clarke A, Pullin R, Bradshaw T, Cole P, Holford KM. Determination of rolling

element bearing condition via acoustic emission. Proc. Inst. Mech. Eng. Part J J. Eng. Tribol., vol. 230, 2016, p. 1377–88. doi:10.1177/1350650116638612.